Science Journal of Chemistry
2025, Vol. 13, No. 1, pp. 11-32
https://doi.org/10.11648/j.sjc.20251301.12

Research Article

Synthesis, Experimental Characterizations and Theoretical Study of the Chemical Reactivity of Coumarin-6-yl Acetate in Gas and Solvent Phases

Honoré Kouadio Yao[1], Zakaria Koulabiga[2], Akoun Abou[1, *], Abdoulaye Djandé[2], Stéphane Coussan[3], Olivier Ouari[4]

[1]Department of Training and Research in Electrical and Electronic Engineering, Research Team: Instrumentation, Image and Spectroscopy, Felix Houphouet-Boigny National Polytechnic Institute, Yamoussoukro, Côte d'Ivoire

[2]Laboratory of Molecular Chemistry and Materials, Research Team: Organic Chemistry and Phytochemistry, University Joseph KI-ZERBO, Ouagadougou, Burkina Faso

[3]Laboratory of Physics of Ionic and Molecular Interactions, National Center for Scientific Research, Aix-Marseille University, Marseille, France

[4]Institute of Radical Chemistry, National Center for Scientific Research, Aix-Marseille University, Marseille, France

Abstract

The first objective of the study is based on experimental characterization of the studied compound. The synthetization process of C11H8O4 (I) involved the *O*-acetylation of 6-hydroxycoumarin with acetic anhydride, utilizing diethyl ether as a solvent and pyridine as a base. The obtained structure was characterized by both spectroscopic analyses such as ESI-MS, FT-IR, ^{1}H and ^{13}C NMR analysis and by single-crystal X-ray diffraction studies. In the latter case, we employed direct methods to solve the structure of (I) and subsequently refined to a final R value of 0.054 for 1896 independent reflections. In the structure, C—H ··O hydrogen bonds connect the molecules into $R_2^2(8)$ dimers, which are linked together by C—H ··O interactions, forming layers parallel to the bc crystallographic plane. Similarly, the crystal structure is sustained by π–π interactions between neighboring rings, with inter-centroid distances lower than 3.8 Å. The second objective of the study is to use theoretical calculation methods to analyze the effect of solvent polarity on the energy gap of the boundary molecular orbitals and the overall chemical reactivity of coumarin-6-yl acetate in order to provide a better understanding of stability and reactivity. A series of density functional theory computations were achieved with B3LYP/6-311^{++}G(d,p) basis set in both gas and solvent phases. In addition to the dipole moment, the natural bond orbital charge distribution was estimated in toluene, tetrahydrofuran (THF) and benzene solvents. The calculations were conducted utilizing the Gaussian 09 software, and the outcomes exhibited that the solvents have an influence on the optimized parameters. Furthermore, dual and local reactivity indices as Fukui functions from the natural bond orbital (NBO) charges were estimated in order to have a better comprehension of the electrophilic and nucleophilic regions, as well as the chemical activity of (I). The obtained dipole moment in the gas phase is 6.03 Debye and those in the presence of the solvents are 7.89, 6.87, 7.51 and 6.83 Debye for water, toluene, THF and benzene, respectively. Additionally, the global chemical reactivity parameters exhibit variation contingent on the molecular compound and polarity of the solvents, making this an important consideration in the selection of appropriate solvents for a given chemical reaction. The studied compound shows higher stability in the benzene solvent evidenced by an E_{HOMO}-E_{LUMO} energy gap of 9.48 eV, while its low stability is observed in the gas phase with an E_{HOMO}-E_{LUMO} energy gap of 6.64 eV.

*Corresponding author: abouakoun@gmail.com (Akoun Abou)

Received: 23 December 2024; **Accepted:** 9 January 2025; **Published:** 24 January 2025

Keywords

Coumarin Ester, Crystal Structure, Spectroscopic Analysis, Quantum Chemical Calculations, Fukui Functions

1. Introduction

Coumarin is a sweet-smelling substance naturally present in many plants, such as cinnamon and tonka bean. Its derivatives have been identified in various plants that are frequently utilized as licorice flavorings. These plants include, but are not limited to, fennel, aniseed, and licorice root [1-3]. Coumarin has been utilized as a flavoring agent in the food and cosmetics industry for a considerable duration. Despite its continued employment in the cosmetics industry, its utilization has been discontinued in the food industry due to the potential for toxic and deleterious effects on the liver [4, 5]. However, low exposure to this naturally occurring compound is expected and should not present a health risk. The Canadian Food Inspection Agency (CFIA) considered it important to examine coumarin levels in common products such as ground cinnamon, cinnamon-containing products and licorice-flavored products to ensure that they are safe for consumption. The Acceptable Daily Intake (ADI) for coumarin is set at 0.1 mg by the European Food Safety Authority (EFSA) in 2004 [6]. Furthermore, coumarin derivatives remain a significant area of interest for organic and medicinal chemists, with a wide range of applications in fragrances, pharmaceuticals, and agrochemicals. They are essential scaffolds for numerous therapeutic compounds, including those with antimicrobial [7], antioxidant, [8] and anti-inflammatory properties [9]. In a similar vein, certain noncentrosymmetric coumarin derivatives find application in the realm of cutting-edge research in domains such as optical communications, optical computing, dynamic imaging, and data storage. These derivatives offer a plethora of advantageous characteristics, including the phenomenon of photoswitching. Extensive research has been conducted to identify novel materials with enhanced nonlinear optical (NLO) properties. This research has been conducted either experimentally or guided by theoretical calculations, with the objective of synthesizing more effective photon-manipulating materials [10-15].

In the present work, the first objective is to elucidate the synthesized structure through both spectroscopic analyses such as ESI-MS, FT-IR, ^{1}H and ^{13}C NMR analysis, and single-crystal X-ray diffraction (XRD) studies [16]. The 3D structure, as determined by X-ray analysis, has been subjected to further analysis through the Multipurpose Crystallographic Tool PLATON [17]. The second objective is to investigate frontier molecular orbital (FMO) energies and derive global reactivity indices in both gas and solvent phases, underpinned by density functional theory (DFT) implemented in Gaussian09 [18]. Furthermore, natural bond orbital (NBO) charges and Fukui Functions (FFs) were calculated to determine the atomic charge distribution for the purpose of identifying electrophilic and nucleophilic areas of the Coumarin-6-yl acetate using the B3LYP/6-311^{++}G(d,p) basis set of Gaussian or the Perdew-Wang (PWC) functional and DND (Double-numerical + d-DNP) basis set of the DMol^{3} module implemented in Materials Studio software [19, 20].

2. Experimental and Theoretical Methods

2.1. Synthesis

The reaction is an *O*-acetylation of 6-hydroxycoumarin with acetic anhydride in the presence of diethyl ether as solvent and pyridine as base. In this reaction, we exploited the HSAB theory which recommends that in acylation with anhydride or aliphatic acyl groups RCO^{+}, which are known to be soft acids, best results are obtained by using soft bases like pyridine [21, 22].

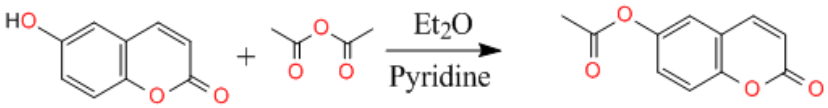

Figure 1. *Synthesis of the title compound. Reagents and conditions: Pyridine, Diethyl ether, room temperature, 3 h.*

The synthesis of the studied compound is analogous to the method described by Abou et al. (2021) [23]. A 100 mL round-necked flask equipped with a water condenser was employed in the successive steps of the reaction. The following reagents were introduced successively: dried diethyl ether (25 mL), acetic anhydride (0.65 mL; 6.17 mmol), and

dried pyridine (2.35 mL; 4.7 molar equivalents). While stirring vigorously, 6-hydroxycoumarin (1 g; 6.17 mmol) was added in small portions over 30 minutes. The reaction mixture was left to stir at room temperature for 3 hours. The mixture was then poured in a separating funnel containing 40 mL of chloroform and washed with diluted hydrochloric acid solution until the pH was 2–3. The organic phase was extracted, washed with water to neutrality, dried over magnesium sulfate ($MgSO_4$) and the solvent removed. The resulting precipitate was filtered off with suction, washed with hexane and recrystallized from chloroform to obtain colorless needle-like crystals of the title compound: yield 72%; M.p. 371-373 K.

2.2. Spectroscopic Spectra Collection

The spectra were collected using the equipment used by abou et al. (2021) [23]. The protocols are the same and are described as follows.

2.2.1. Electrospray Ionization Mass Spectrum

The analyses were conducted on a 3200 QTRAP spectrometer (Applied Biosystems SCIEX) furnished with a pneumatically abetted air pressure ionization (API) source for ESI-MS^+ experiment. The sample in solution was ionized under the following conditions: electrospray tension (ISV): 5500 V; orifice tension (OR): 20 V; nebulizing gas pressure (air): 10 psi. The mass spectra (Figures 2 and 3) were attained with a quadrupole analyzer.

2.2.2. ATR-FTIR Spectrum

The infrared spectrum (Figure 4) was analyzed using a Bruker IFS 66/S Fourier Transform Infrared (FTIR) spectrometer, which was operated by the OPUS 6.5 software and employed the attenuated total reflectance (ATR) technique with a germanium tip. The absorption bands in the range 4000-400 cm^{-1} are expressed in wavenumber $\bar{\upsilon}$ (cm^{-1}): resolution 1 cm^{-1}, 300 scans.

2.2.3. NMR Spectra

^1H and ^{13}C-NMR spectra (Figures 5 and 6) were performed on a Bruker AMX-400 spectrometer at 300 and 100 MHz respectively, utilizing TMS as internal standard (chemical shifts in δ ppm, coupling constants J in Hz) and deuterated chloroform ($CDCl_3$) as a solvent.

The ^{13}C spectrum was gained from an APT (Attached Proton Test) experiment.

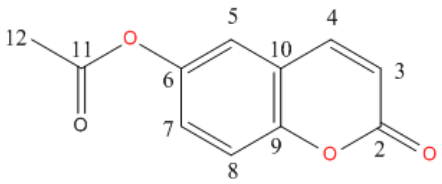

Figure 2. *Numbering of carbon atoms used in spectra analysis.*

2.3. Crystal Structure Analysis

Diffraction intensities for Coumarin-6-yl Acetate were measured on Rigaku Oxford Diffraction SuperNova, Dual, Cu at zero, AtlasS2 diffractometer [24] utilizing a mirror monochromator and Cu *K*α radiation (λ = 1.54184 A) at 298 K. The structure was determined by direct methods utilizing SIR 2014 [25] incorporated in the WinGX [26] program suite. The refinement of the resolved structure was made by full-matrix least squares method on the positional and anisotropic temperature parameters of the non-hydrogen atoms, using 137 crystallographic parameters, with SHELXL2014 program [27]. All H atoms were placed in calculated positions with [C—H = 0.93 Å (aromatic), 0.96 Å (methyl)] and refined using a riding model approximation with U_{iso}(H) constrained to 1.2 times U_{eq}(C-aromatic) or 1.5 times U_{eq}(C-methyl) of the respective parent atom. Data collection, cell refinement and data reduction are by CrysAlis PRO [23, 24]. The universal crystallographic tool PLATON was utilized to analyze the structure and present the results. Specifics information of the data acquisition conditions and the parameters of the refinement process are presented in Table 1.

2.4. Theoretical Computational Procedures

The optimized structure of the coumarin ester was performed via the density functional theory (DFT) implemented in the Gaussian 09W software package developed by Frisch and coworkers, using the job type Opt+Freq and restricted exchange correlation functional (RB3LYP) as calculation method with the 6-311^{++}G(d,p) basis set in the ground state due to its accurate computational results on geometric and energetic parameters [28]. Subsequent calculations are conducted using the M062X method with the 6-311^{++}G(d,p) basis to estimate the electronic properties of this compound, such as ionization potential (I), electronic affinity (A), lowest unoccupied molecular orbital (LUMO), highest occupied molecular orbital (HOMO) and energy gap (ΔE_g). In addition, Koopman's theorem for closed-shell molecules is used to compute the various global chemical reactivity descriptors in diverse types of solvents. Fukui functions, natural bond orbital (NBO) charges, and thermodynamic parameters can be calculated and discussed [29-34]. All the output files originating from the calculations were visualized by the Gaussian View 06 program and the module $DMol^3$ implemented in Materials Studio software.

3. Results and Discussion

3.1. Spectra Analysis

3.1.1. Interpretation of Electrospray Ionization Mass Spectrum

As illustrated in Figures 3 and 4, the peak observed at m/z

205 due to the pseudo-molecular ion $[M+H]^+$ is consistent with the molecular weight of 204 $g.mol^{-1}$, which is in accordance with the chemical formula $C_{11}H_8O_4$.

ESI-MS m/z 205 ($[M+H]^+$)

ESI-MS/MS m/z (%): 205 (MH^+, 25), 163.2 (100), 135.2 (4.5), 119.0 (1.8 weak), 107.2 (3.6), 91.2 (1 weak), Figure 3.

3.1.2. Infrared Spectrum

For the studied compound, the FTIR spectrum showed absorption bands at 3224.1 cm^{-1} (C-H, aromatic), 2982.7 cm^{-1} (C-H, aliphatic), 1741.4 cm^{-1} and 1672.4 cm^{-1} for the two carbonyls, 1241.4 cm^{-1} (C–O–C, lactone), and 1086.2 cm^{-1} (C–O–C, ester). C=C signals were in the range of 1448.3 cm^{-1} to 1639.7 cm^{-1}, (Figure 5) [23].

3.1.3. ^{1}H-NMR Spectrum

The analysis (chemical shifts and coupling constants) of the ^{1}H NMR spectrum (Figure 6) highlighted five spots, four of which were in the range 6-8.5 ppm and due to aromatic hydrogens. The three equivalent methyl protons are clearly visible at 2.3 ppm.

^{1}H-NMR ($CDCl_3$, 400 MHz, δ ppm): 7.6 (d, 1H, J = 9.6 Hz, H-4); 7.4 (m, 1H, H-5); 7.3 (m, 2H, H-7 and H-8); 6.4 (d, 1H, J = 9.6 Hz, H-3); 2.3 (s, 3H, H-12).

3.1.4. ^{13}C (APT)-NMR Spectrum

In NMR studies, an APT sequence is employed to detect attached protons: CH3 and CH signals are positive, whilst CH2 and quaternary carbons signals are negative.

As illustrated in Figure 7, the APT spectrum of the molecule consists of 11 signals, in line with expectations. Six positive peaks were observed, suggesting the presence of five aromatic tertiary carbons and the shielded primary carbon of a methyl group. In contrast, five peaks were inverted, indicating quaternary carbons (C-2, C-6, C-9, C-10 and C-11).

^{13}C (APT)-NMR ($CDCl_3$, 100 MHz, δ ppm): 169.5 (C-11), 160.6 (C-2), 151.8 (C-6), 146.9 (C-9), 142.9 (C-4), 125.5 (C-8), 120.3 (C-7), 119.4 (C-10), 118.1 (C-5), 117.7 (C-3), 21.2 (C-12).

3.1.5. Heteronuclear Single-Quantum Correlation (HSQC) NMR Spectrum

As illustrated in Figure 8, the HSQC-NMR spectrum displayed six peaks demonstrating a strong correlation between the primary carbon C-12 and the methyl protons, as well as between each tertiary carbon (C-3, C-4, C-5, C-7, C-8) and the proton directly attached via 1JC-H scalar coupling. The spots obtained through this analysis confirm the previously identified signals in the ^{1}H and ^{13}C (APT)-NMR spectra.

3.1.6. Conclusion of Spectra Analysis

The results of the spectrometric analysis, when superimposed, corroborate the molecule illustrated in Figure 2. Other investigative methods, including X-ray and theoretical calculations, have been employed to validate this conclusion [35, 36].

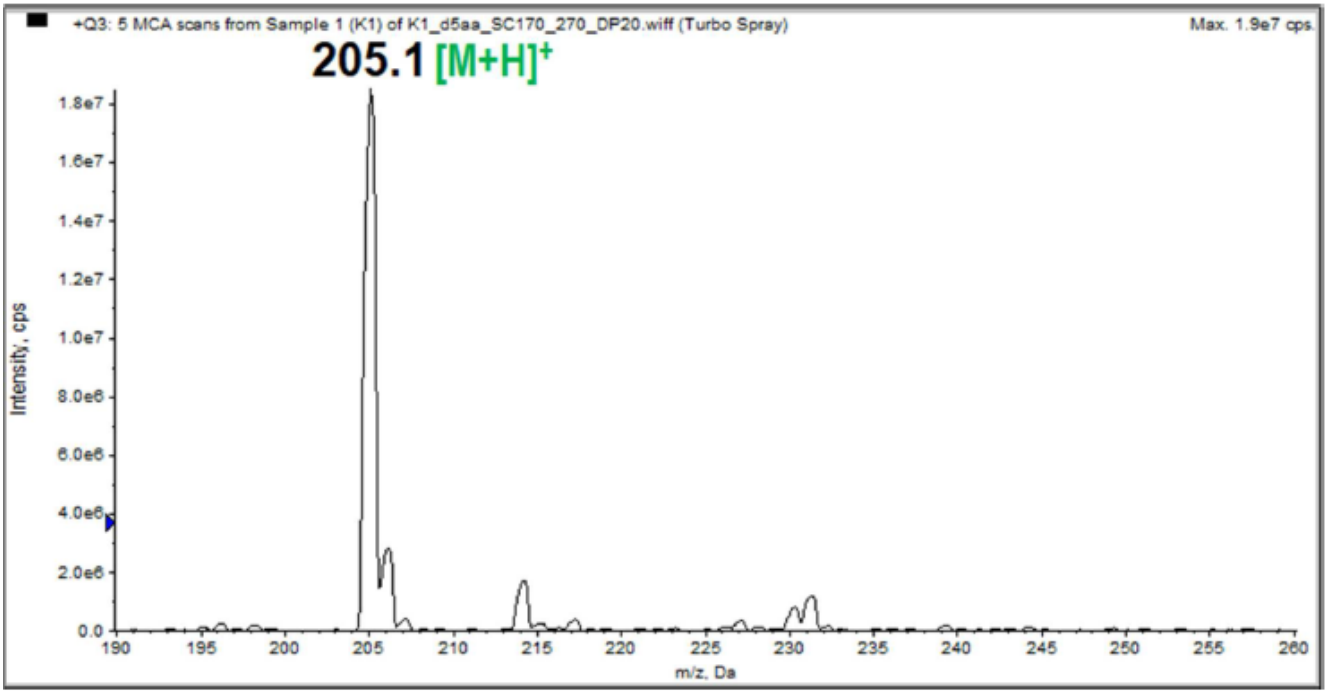

Figure 3. *Electrospray ionization mass spectrum of the studied sample.*

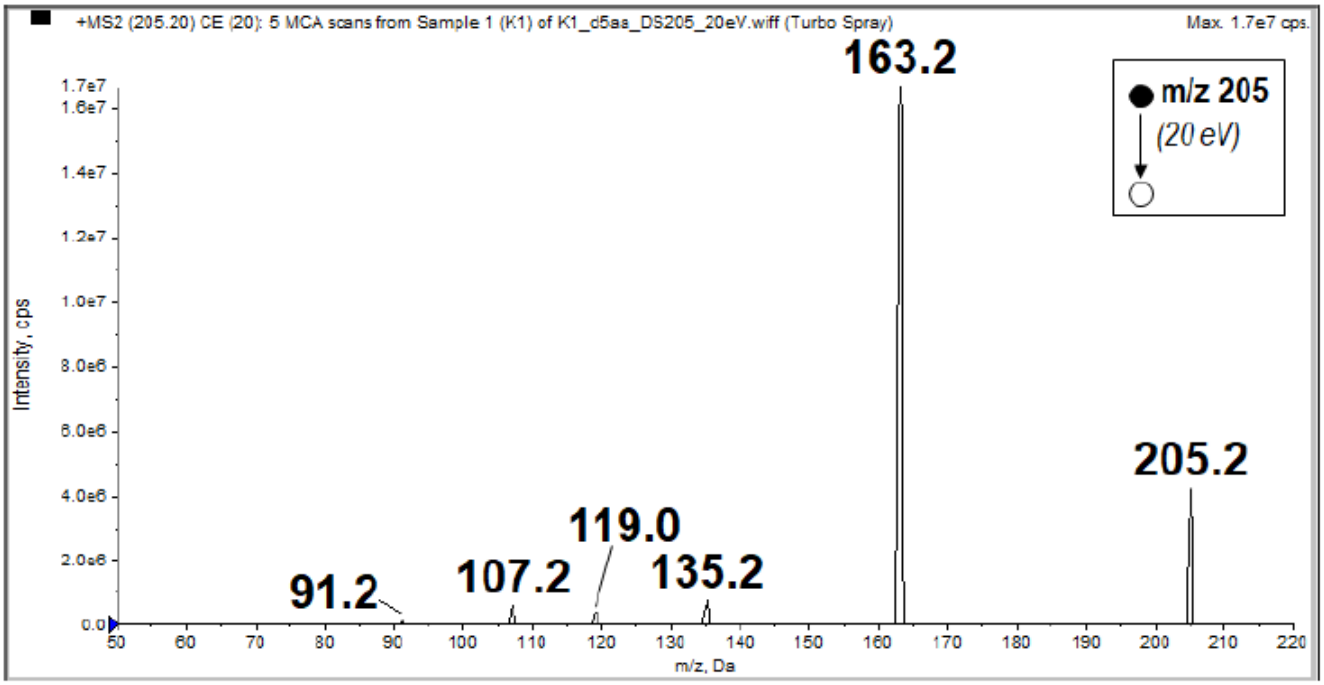

Figure 4. *MS/MS spectrum of the protonated molecular ion peak (MH^+) at m/z 205.*

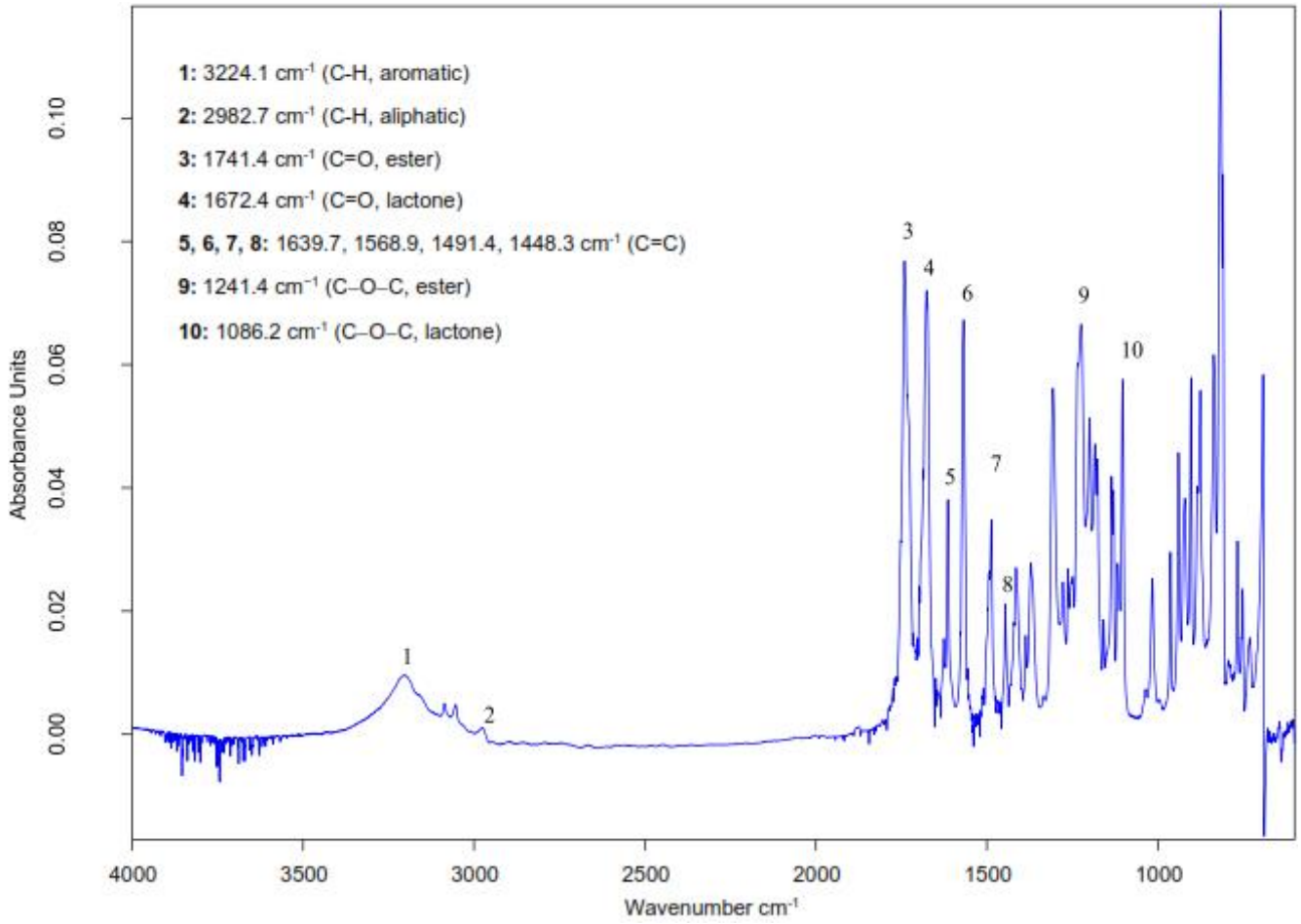

Figure 5. *Experimental ATR-FTIR Spectrum.*

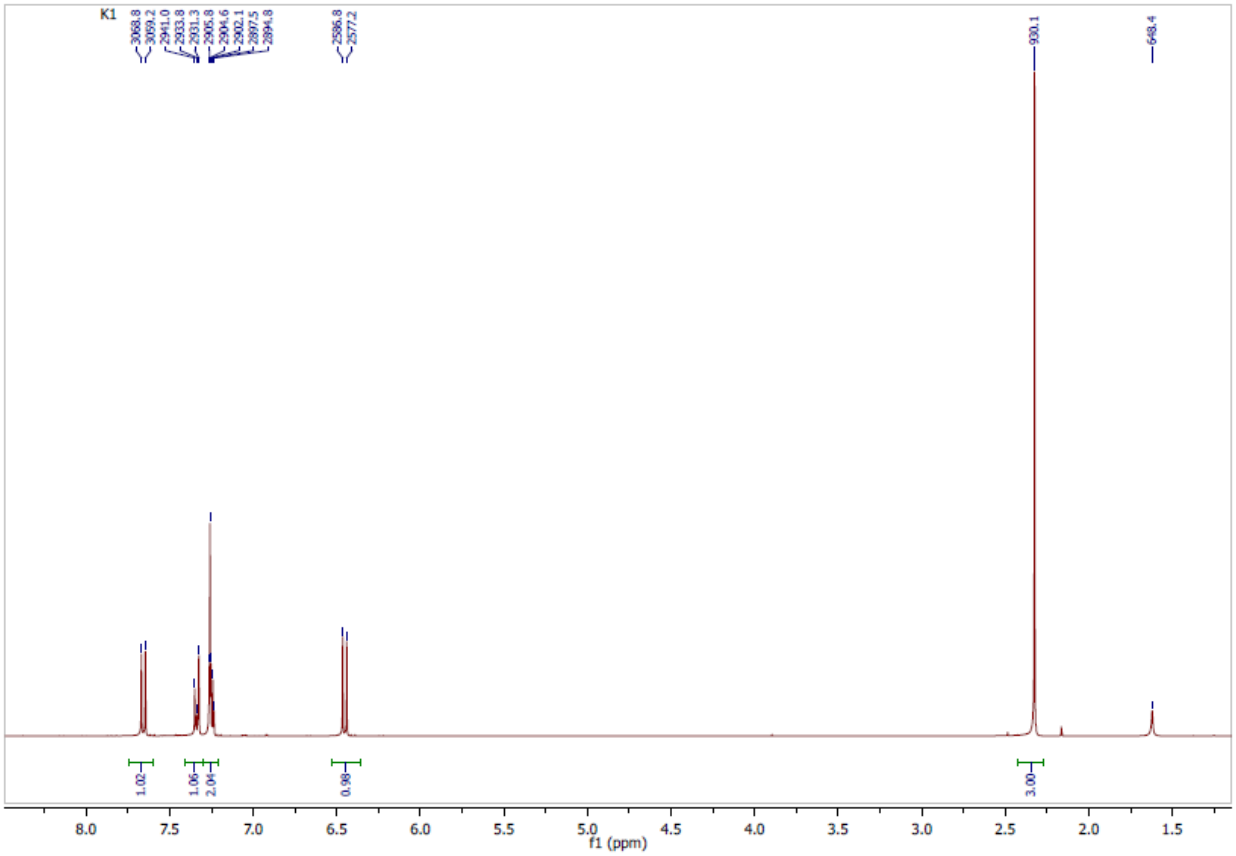

Figure 6. *Experimental ^{1}H-NMR Spectrum: $CDCl_3$, 300 MHz.*

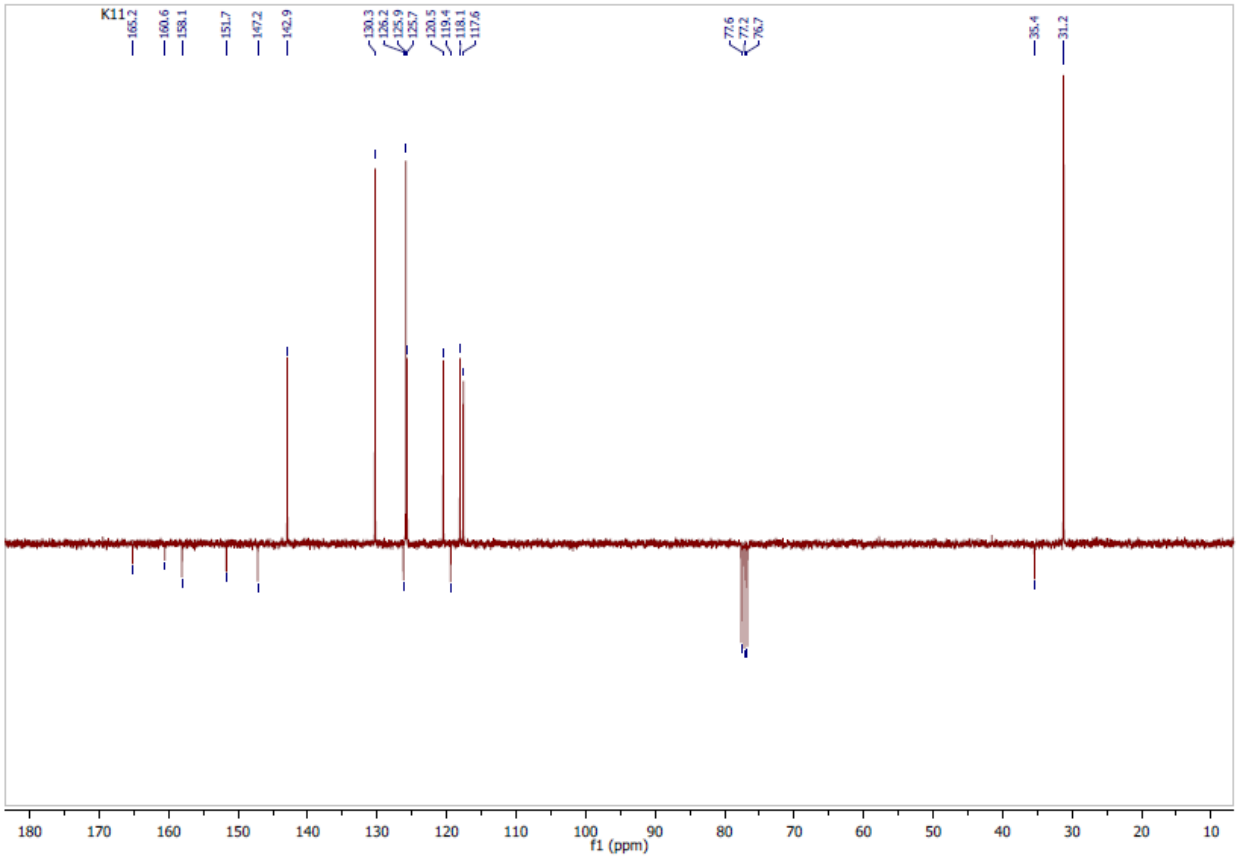

Figure 7. *Experimental ^{13}C (APT)-NMR Spectrum: $CDCl_3$, 100 MHz.*

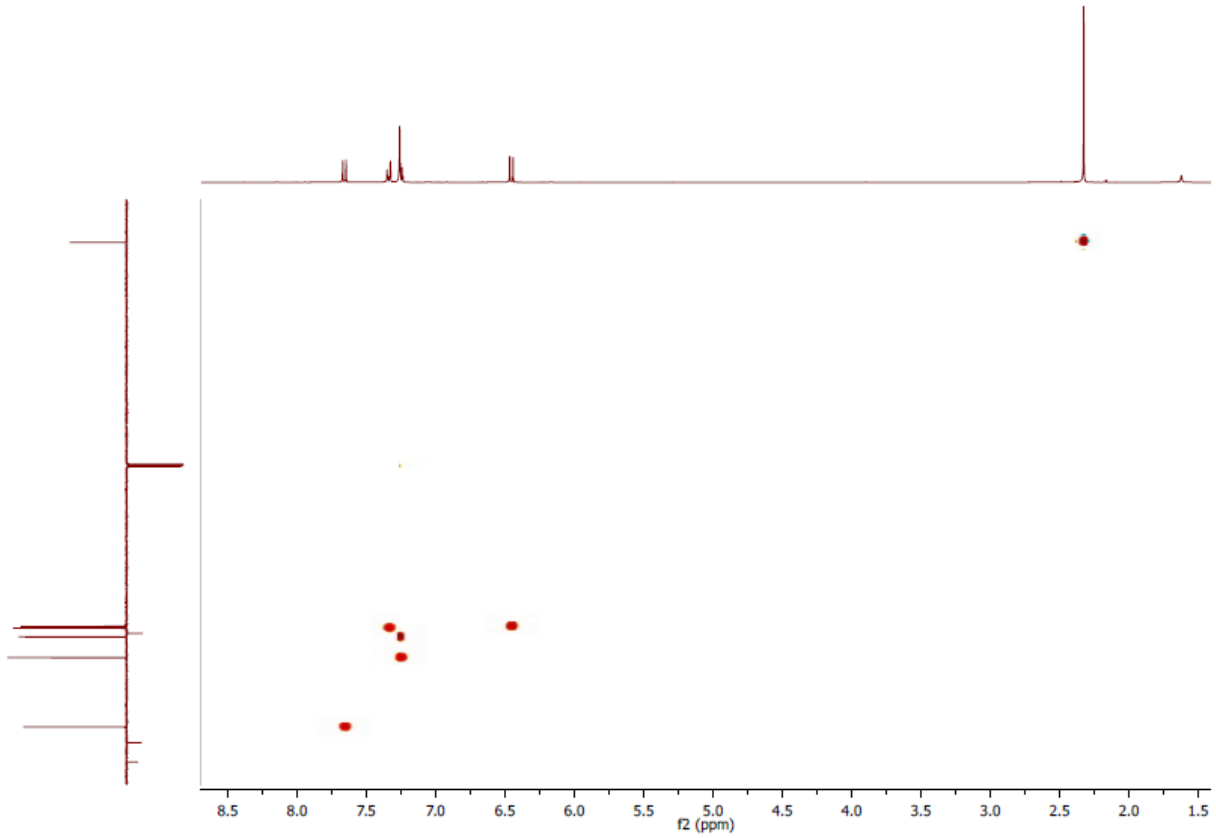

Figure 8. *Experimental HSQC Spectrum: $CDCl_3$, ^{1}H-NMR 300 MHz; ^{3}C (APT)-NMR 100 MHz.*

3.2. Structural Description

3.2.1. Structural Commentary

The structural configuration of the title compound (Figure 9) is characterized by a planar conformation of the coumarin ring system, as evidenced by the Puckering analysis parameter tau (τ=0.7°), which is less than 5°, the maximum value considered indicative of an effective planar conformation [17].

A thorough analysis of the bond lengths indicates a slightly uneven distribution around the pyrone ring. The C2-C3 bond length (1.340(2) Å) and the C1-C2 bond length (1.451(2) Å) exhibit a shorter and longer deviation, respectively, from the expected Car-Car bond length. This finding suggests that the electron density is less concentrated in the C2-C3 bond of the pyran-2-one ring, which results in the formation of a double bond, as reported in other coumarin ester derivatives [37-39].

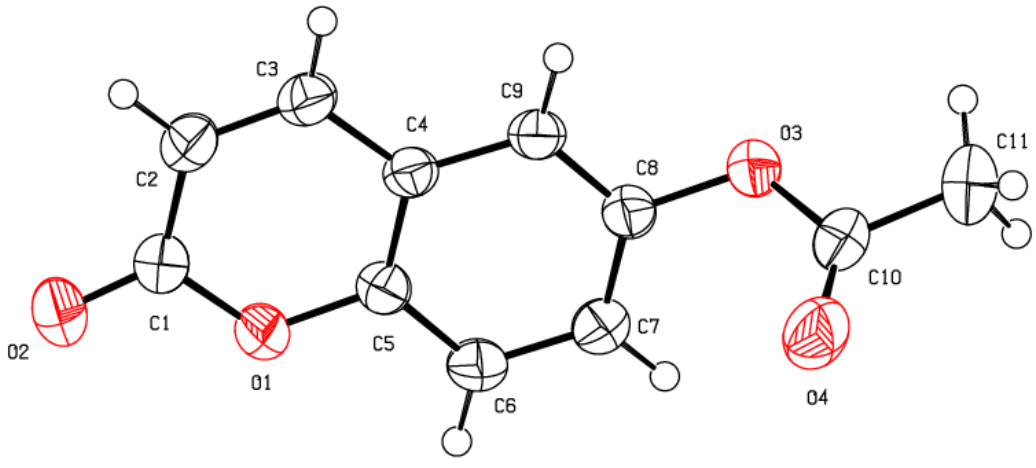

Figure 9. *An ORTEP view of the title compound (I) with the atomic numbering scheme. Displacement ellipsoids are shown at the 50% probability level.*

Table 1. *Crystal data and details of the structure determination.*

chemical formula	$C_{11}H_8O_4$	Theta range for data collection [°]	7.1 - 76.2
Formula weight	204.17	Crystal size [mm^3]	0.28 × 0.28 × 0.04
Temperature [K]	298	Index ranges	-4 ≤ h ≤4; -46 ≤ k ≤ 47; -8 ≤ l ≤ 8
Wavelength λ [Å]	1.54184	Reflections collected	8017
Crystal system	Monoclinic	Absorption coefficient [mm^{-1}]	0.96
Space group	$P2_1/n$	Theta full [°]	67.684
Unit cell dimensions		F(000)	424
a [Å]	3.9039(2)	Refinement method	Full-matrix least squares on F^2
b [Å]	37.5379(12)	Data/restraints/parameters	1712/0/ 136
c [Å]	6.4621(3)	Goodness of fit	1.03
α [°]	90	Final R indices [$F^2 > 2.0\ \sigma(F^2)$]	R_1 = 0.055, wR_1= 0.164
β [°]	103.726(4)	Density calculated [$g.cm^{-3}$]	1.265
γ [°]	90	Independent reflections	1896
Volume [$Å^3$]	919.94(7)	R_{int}	0.032
Z	4	R indices (all data)	0.0574
Crystal description	plate	$\Delta\rho_{max}$, $\Delta\rho_{min}$ (e $Å^{-3}$)	0.28, -0.17
crystal color	Colorless	$(\Delta/\sigma)_{max}$	< 0.001
Diffractometer	SuperNova, Dual, Cu at zero, AtlasS2	Absorption correction	multi-scan; CrysAlisPro 1.171.42.79a (Rigaku Oxford Diffraction, 2022) Empirical absorption correction using spherical harmonics, implemented in SCALE3 ABSPACK scaling algorithm.

3.2.2. Supramolecular Features

The crystal structure reveals the generation of $R_2^2(8)$ dimeric units via C—H ··O interactions. These dimers are linked together by non-classical hydrogen bonds through C—H ··O, forming chains in the bc plane (Figure 10). Similarly, aromatic π-π stacking interactions have been observed between adjacent coumarin and pyrone rings, with centroid-centroid distances measuring less than 3.8 Å. This distance is considered to be the maximum threshold for effective π-π interaction [40]. These aromatic interactions are present and link the dimers (Figure 11), (Table 3). The collective contribution of these molecular interactions is instrumental in ensuring the stable assembly of three-dimensional crystals.

For convenience, we have provided a summary of the perpendicular distances of Cg(I) on the J ring and the distances between Cg(I) and the perpendicular projection of Cg(J) on the I ring (slip) in Table 3.

Table 2. *Hydrogen-bond geometry (Å,).*

D—H…A	D—H	H…A	D…A	D—H…A
C2—H5…O2^{i}	0.93	2.51	3.397 (2)	160
C11—H11C…O4^{ii}	0.96	2.58	3.378 (2)	141

Symmetry code: (i) 2−*x*, −*y*, −*z*; (ii) -1/2+*x*, 1/2-*y*, 1/2+*z*.

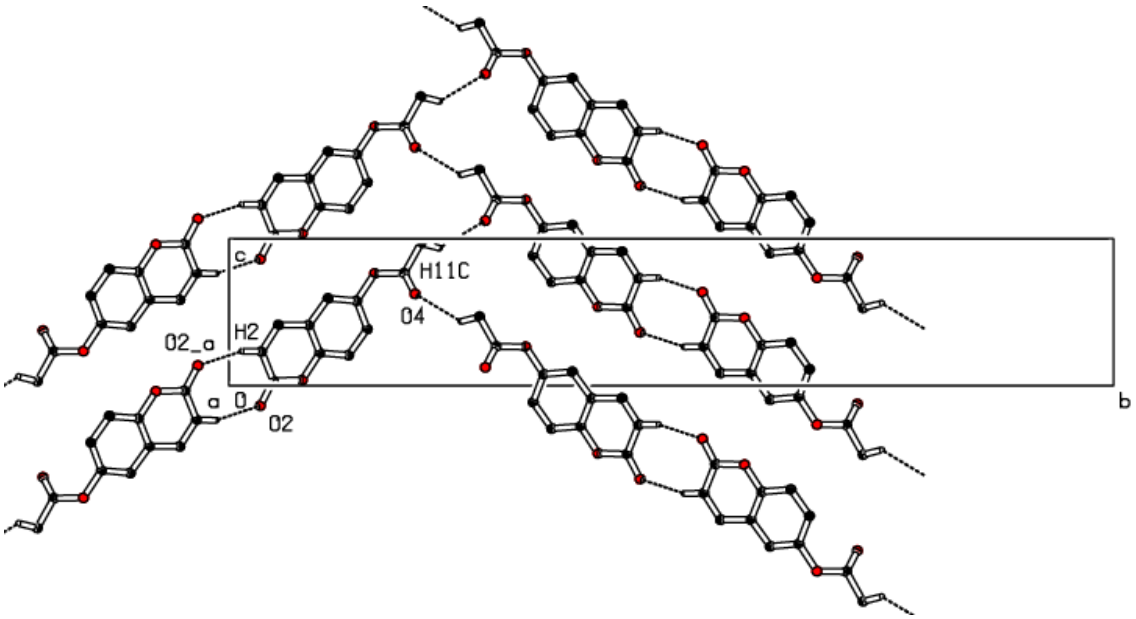

Figure 10. *A view of the crystal packing, showing C—H ··O hydrogen bonds linking molecules into* $R_2^2(8)$ *dimeric units and their propagation into the bc plane.*

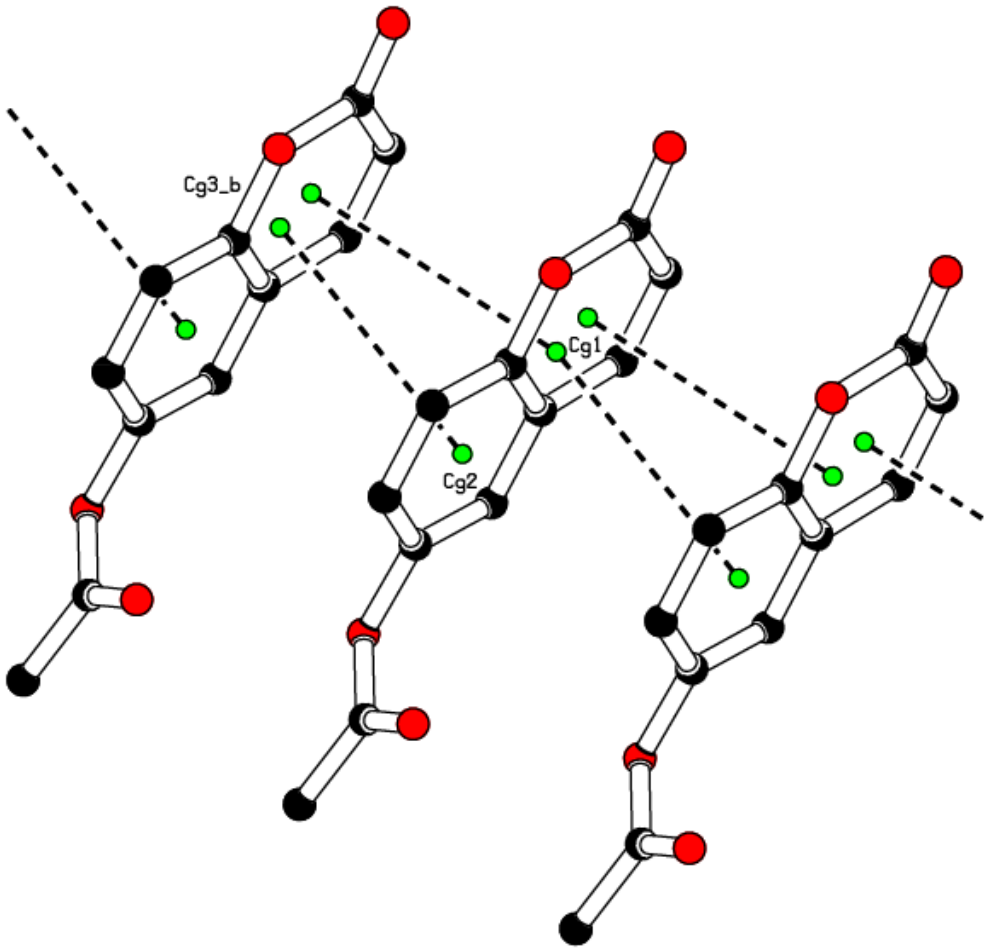

Figure 11. *π···π stacking interactions in the crystal packing.*

Table 3. *Analysis of short ring interactions (Å). Cg1 and Cg3 are the centroids of the pyrone and the coumarin rings, respectively. The distances between the centroid of ring I and its perpendicular projection on ring J, as well as the distances between the centroid of ring I and the perpendicular projection of ring J on ring I (slippage), are reported.*

Cg(I)	Cg(J)	Symmetry Cg(J)	Cg(I)…Cg(J)	CgI_Perp	CgJ_Perp	Slippage
Cg1	Cg3	1+x, y, z	3.7192(8)	-3.4080 (6)	3.4147 (5)	1.474
Cg2	Cg3	-1+x, y, z	3.7226 (8)	3.4061 (6)	-3.4004 (5)	1.515

Table 4. *Fractional atomic coordinates and isotropic or equivalent isotropic displacement parameters (Å^2).*

Atom	x	y	z	U_{eq}
O1	0.5293 (3)	0.08275 (3)	0.03878 (15)	0.0436 (3)
O2	0.6298 (4)	0.03526 (3)	−0.13667 (18)	0.0603 (4)
O3	0.7013 (3)	0.79975 (19)	0.76450 (16)	0.0434 (3)
O4	0.61611 (4)	0.21027 (3)	0.6250 (2)	0.0677 (4)
C1	0.6875 (4)	0.04991 (4)	0.0338 (2)	0.0429 (4)
C2	0.9057 (4)	0.03680 (4)	0.2330 (2)	0.0446 (4)
C3	0.9557 (4)	0.05577 (4)	0.4134 (2)	0.0415 (4)
C4	0.7911 (4)	0.09011 (3)	0.4138 (2)	0.0348 (3)
C5	0.5812 (4)	0.10251 (3)	0.2228 (2)	0.0360 (3)
C6	0.4105 (4)	0.13520 (4)	0.2078 (2)	0.0420 (4)
C7	0.4547 (4)	0.15620 (4)	0.3872 (2)	0.0414 (4)
C8	0.6686 (4)	0.14433 (3)	0.5779 (2)	0.0367 (3)
C9	0.8354 (4)	0.11183 (4)	0.5949 (2)	0.0376 (3)
C10	0.8350 (4)	0.19810 (4)	0.7676 (2)	0.0424 (4)
C11	0.8240 (5)	0.21674 (5)	0.9701 (3)	0.0575 (5)

Table 5. *Experimental and DFT/ RB3LYP/6-311^{++}G(d,p) calculated bond lengths in (Å) for compound (I).*

Bond	X-Ray	Calc.(gas)	Bond	X-Ray	Calc.(gas)	Bond	X-Ray	Calc.(gas)
O1—C5	1.375 (2)	1.366	C5—C4	1.390 (2)	1.404	C8—C9	1.375 (2)	1.380
O1—C1	1.383 (2)	1.391	C4—C9	1.403 (2)	1.406	C9—C4	1.403 (2)	1.406
O3—C10	1.358 (2)	1.374	C3—C2	1.340 (2)	1.350	O2—C1	1.204 (2)	1.207
O4—C10	1.192 (2)	1.202	C4—C3	1.441 (2)	1.440	C10—C11	1.494 (2)	1.502
O3—C8	1.407 (2)	1.398	C6—C7	1.379 (2)	1.387	C1—C2	1.451 (2)	1.456
C5—C6	1.389 (2)	1.394	C7—C8	1.388 (2)	1.397			

Table 6. *Experimental and DFT/ RB3LYP/6-311^{++}G(d,p) calculated bond angles (°) for compound (I).*

Bond angle	X-Ray	Calc.(Gas)	Bond angle	X-Ray	Calc.(Gas)	Bond angle	X-Ray	Calc.(Gas)
C5—O1—C1	121.72 (11)	122.85	O1—C5—C4	121.53 (12)	121.37	C2—C3—C4	120.19 (13)	120.71
C10—O3—C8	117.99 (11)	119.20	C6—C5—C4	121.99 (13)	121.10	O2—C1—O1	116.16 (14)	115.87
C8—C9—C4	119.07 (12)	119.82	C6—C7—C8	119.46 (13)	119.75	O2—C1—C2	126.91 (14)	126.22
C5—C4—C9	118.47 (13)	118.72	C3—C2—C1	121.76 (14)	121.76	O1—C1—C2	116.93 (13)	115.87
C5—C4—C3	117.86 (12)	117.44	C9—C8—C7	122.06 (13)	121.12	O4—C10—O3	123.35 (14)	123.52
C9—C4—C3	123.67 (12)	123.83	C9—C8—O3	117.82 (12)	117.67	O4—C10—C11	125.86 (15)	125.72
C7—C6—C5	118.95 (13)	119.49	C7—C8—O3	119.99 (13)	121.09	O3—C10—C11	110.79 (13)	110.76
O1—C5—C6	116.48 (12)	117.53						

Table 7. *Experimental and DFT/ RB3LYP/6-311^{++}G(d,p) calculated dihedral angles (°) for compounds (I).*

Dihedral angles	X-Ray	Calc.(Gas)	Dihedral angles	X-Ray (I)	Calc.(Gas)
C8—C9—C4—C5	0.5 (2)	0.17	C6—C7—C8—C9	−1.0 (2)	-0.23
C8—C9—C4—C3	179.43 (13)	-179.89	C6—C7—C8—O3	−176.70 (13)	-176.10
C1—O1—C5—C6	179.51 (13)	-179.97	C10—O3—C8—C9	123.21 (15)	120.51
C1—O1—C5—C4	−1.0 (2)	-0.090	C10—O3—C8—C7	−60.88 (19)	-63.48
C7—C6—C5—O1	−179.67 (13)	179.82	C1—C2—C3—C4	0.1 (2)	-0.08
C7—C6—C5—C4	0.9 (2)	-0.06	C5—C4—C3—C2	0.1 (2)	0.05
C9—C4—C5—O1	179.35 (12)	179.98	C9—C4—C3—C2	−178.86 (14)	-179.89
C3—C4—C5—O1	0.3 (2)	0.04	C5—O1—C1—O2	−178.57 (14)	-179.99
C9—C4—C5—C6	−1.2 (2)	-0.15	C5—O1—C1—C2	1.2 (2)	0.05
C3—C4—C5—C6	179.74 (13)	179.91	C3—C2—C1—O2	178.99 (17)	-179.91
C5—C6—C7—C8	0.2 (2)	0.25	C3—C2—C1—O1	−0.8 (2)	0.04
C4—C9—C8—C7	0.6 (2)	0.02	C8—O3—C10—O4	−4.4 (2)	-0.41
C4—C9—C8—O3	176.43 (12)	176.03	C8—O3—C10—C11	175.44 (13)	179.69

3.3. Theoretical Calculations

In this study, we will compare the geometrical parameters obtained from theoretical calculations to those originating from x-ray crystallography to check their agreement before estimating the chemical reactivity descriptors.

3.3.1. Comparison of Geometrical Parameters

The geometrical parameters of (I) obtained from theoretical calculations are then confronted with those yielded from the X-ray crystallographic study. The comparison demonstrates a high level of consistency between bond lengths and bond angles, as evidenced by root mean square deviations (RMSD) of 0.01 Å for bond lengths and 0.67 ° for bond angles (Tables 5 and 6). Additionally, analysis of the calculated torsion angles confirms the planarity of the coumarin moiety (Table 7).

The above comparisons demonstrate that the theoretical calculations are in good alignment with the crystallographic predictions based on solid-state structure. Therefore, the calculated structure can be utilized to compute the chemical properties of (I) in solid state.

3.3.2. Molecular Electrostatic Potential (MEP)

Electrostatic interactions in a range of chemical systems

have been extensively described by the MEP [41]. The force exerted on a positive test charge (a proton) positioned above the charge cloud produced by the molecule's electrons and nuclei at any given time is known as the molecular electrostatic potential. Equation (1) was utilized to compute the values for the current system as previously mentioned [42].

$$V(r) = \sum_A \frac{Z_A}{|R_A - r|} - \int \frac{\rho(r')d^3r'}{|r' - r|} \quad (1)$$

Where Z_A denotes the charge of nucleus A situated in R_A, whilst ρ(r') signifies the electron density function of the molecule and r' serves as the dummy integration variable.

Figure 12 shows the color visualizations of the calculations' outcomes in the gaseous state of (I) and in various solvents. Blue coloration indicates higher positive potential, which is advantageous for nucleophilic attack, while red coloration indicates higher negative potential, which is advantageous for electrophilic attack. The figure shows two possible locations for electrophilic attack on the compound in gaseous and solvent media. The negative regions are concentrated on the oxygen atoms O2 and O4, with maximum values of -0.0574 a.u. (gas), -0.0721 a.u. (water), -0.0692 a.u. (THF), -0.0640 a.u. (benzene), and -0.0651 a.u. (toluene). The presence of the intermolecular C2—H5···O2 [2−x, −y, −z] and C11—H11C···O4 [−1/2+x, 1/2−y, 1/2+z] hydrogen bonds is thus confirmed. As for the remaining atoms in the coumarin nucleus, their light blue environment suggests that they constitute electropositive weakening areas.

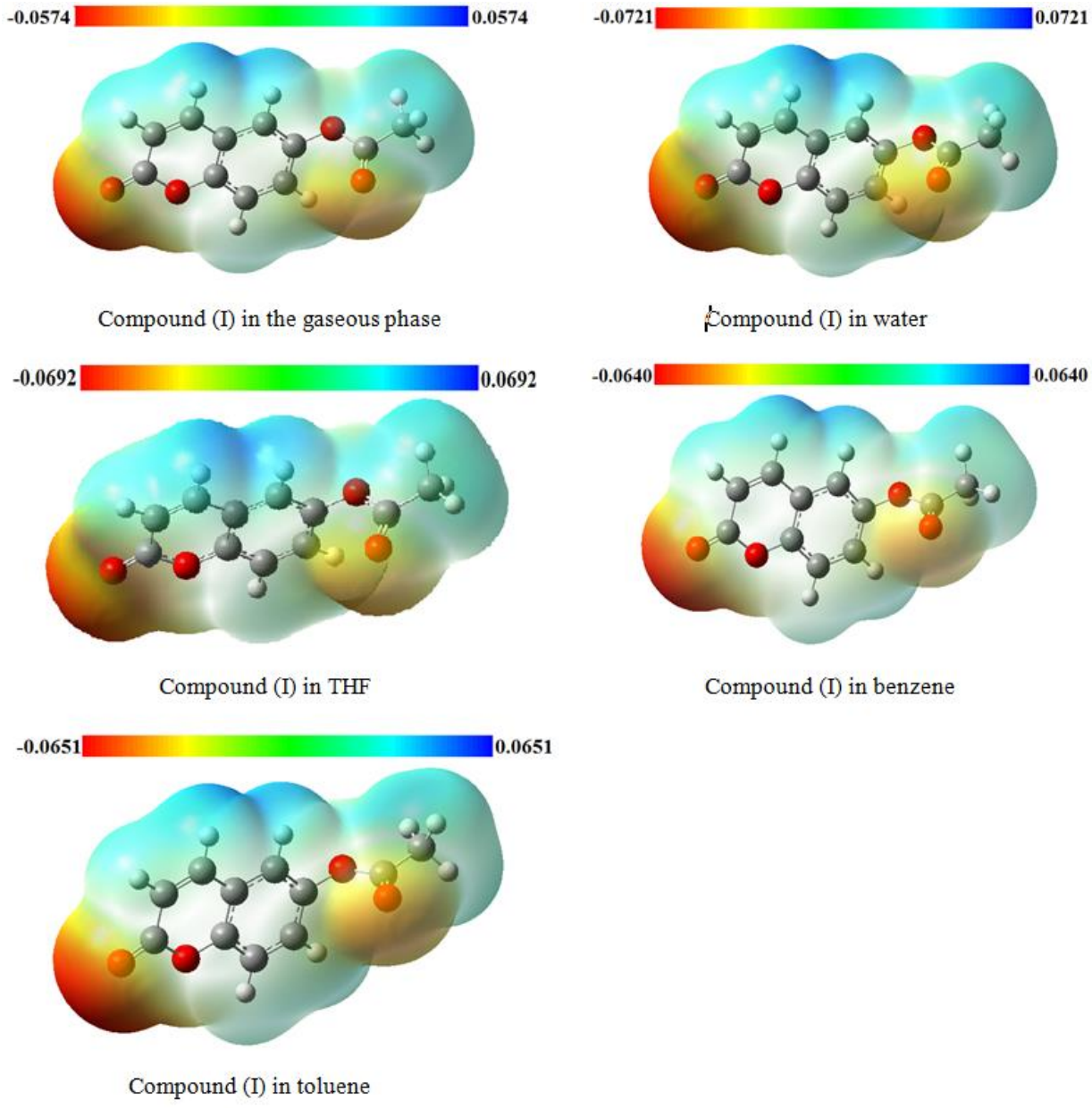

Figure 12. *MEP map (in atomic units) calculated using DFT/ RM062X /6-311++G(d,p).*

3.3.3. Reactivity Descriptors

(i). Global Descriptors

A number of theoretical descriptors, which are related to the conceptual DFT, are utilized in order to determine chemical reactivity forecasts. These include electronegativity (χ), which indicates a molecule's ability to retain its electrons; global softness (σ), which indicates a system's resistance to changes in its electron number; and the overall electrophilicity index (***ω***), which indicates a molecule's electrophilic power. The least vacant molecular orbital energy (E_{LUMO}) is also of significance in this regard, as it describes the sensitivity of the molecule to nucleophilic attack, whilst the highest occupied molecular orbital energy (E_{HOMO}) is important in terms of its description of the molecule's sensitivity to electrophilic attack. The following equations are utilized to calculate these parameters [43]:

$$\Delta E_g = E_{LUMO} - E_{HOMO} \quad (2)$$

$$I = -E_{HOMO} \quad (3)$$

$$A = -E_{LUMO} \quad (4)$$

$$\chi = -\mu = -\frac{E_{LUMO}+E_{HOMO}}{2} \quad (5)$$

$$\eta = \frac{E_{LUMO} - E_{HOMO}}{2} \quad (6)$$

$$\omega = \frac{\mu^2}{2\eta} \quad (7)$$

$$\sigma = \frac{1}{2\eta} \quad (8)$$

Table 8 presents the results of the calculated energetic parameters, which demonstrate that compound (I) in these mixtures are stables. However, compound (I) in the benzene solvent is the most stable with an energy gap value of 9.48 eV, whereas (I) in the gas phase remains the least stable with the lowest energy gap value of 6.64 eV [44]. This is also backed up by the fact that Gaussian did not identify any negative frequencies in its frequency calculation.

Table 8. *Global reactivity descriptors calculated with the DFT/ M062X/6-311^{++}G(d,p) method.*

	Gas	Water	THF	Benzene	Toluene
E_{LUMO} (eV)	-1.48	-1.51	0.74	0.75	-1.51
E_{HOMO} (eV)	-8.12	-8.24	-8.72	-8.73	-8.20
I (eV)	8.12	8.24	8.72	8.73	8.20
A (eV)	1.48	1.51	-0.74	-0.75	1.51
χ (eV)	4.80	4.88	3.99	3.99	4.86
μ (eV)	-4.80	-4.88	-3.99	-3.99	-4.86
η (eV)	3.32	3.37	4.73	4.74	3.35
σ (eV^{-1})	0.151	0.149	0.106	0.105	0.149
ω (eV)	3.470	3.531	1.683	1.679	3.523
ΔE_g (eV)	6.64	6.73	9.46	9.48	6.69

For convenience, Table 8 also shows the overall chemical reactivity indices. From these results, it can be seen that compound (I) in gaseous phase has the lowest overall hardness value (η = 3.32eV). It can therefore be considered as the softest of the series. In contrast, compound (I) in water gives the highest value of electronegativity (χ = 4.88 eV) and electrophilicity index (ω = 3.531 eV), indicating that it is more electron accepting than the Coumarin-6-yl acetate derivative in other solvents.

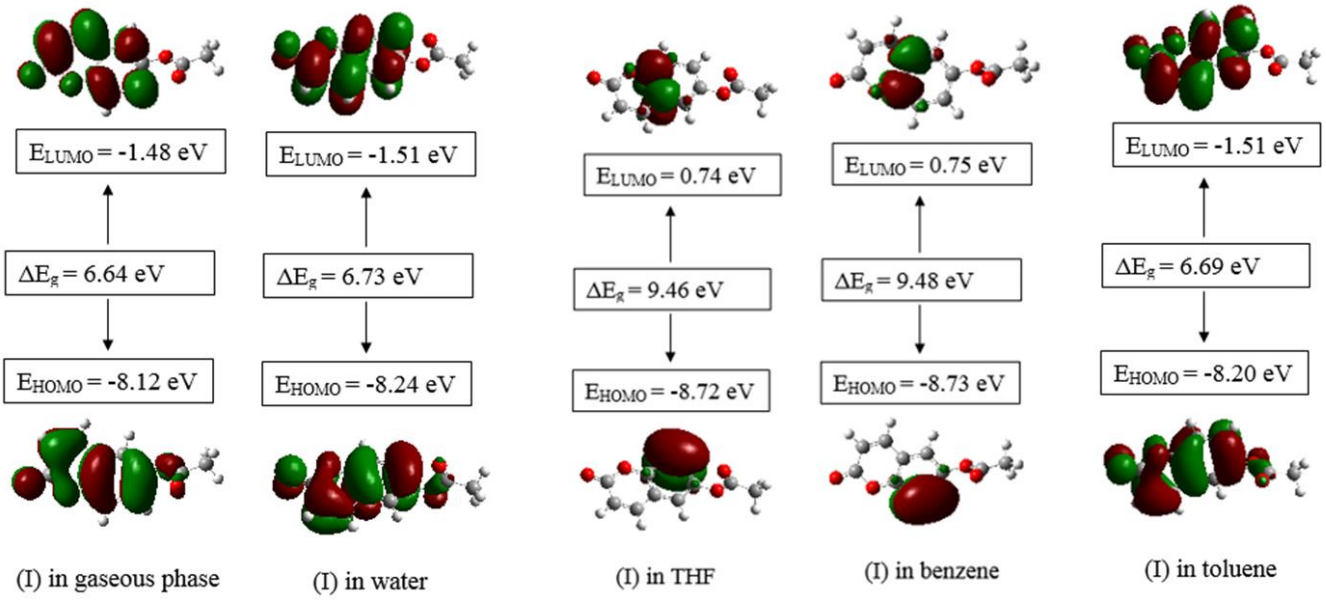

Figure 13. *Calculated HOMO and LUMO orbital distributions and energy levels for the molecule (I) in solvents.*

(ii). Local Descriptors and Dual Descriptors

Various indices have been used to distinguish between the reactive behaviors of the atoms that make up a molecule. These are local and dual descriptors of reactivity at the local level. In this case, the Fukui function (f_k^+, f_k^-) [45], the local softness (σ_k^+, σ_k^-), the local electrophilic power (ω_k^+, ω_k^-), and the dual descriptors have been used to elucidate the electrophilic and nucleophilic selectivity of the molecule. It is essential to note that the Fukui function f_k^+ quantifies reactivity when the molecule is subjected to nucleophilic attack, whereas the Fukui function f_k^- elucidates the electrophilic reactivity of a specific site. The uppermost Fukui function value is attributed to the greatest active location. The condensed indices σ_k^+ and ω_k^+ indicate a site's capacity to gain electron density through nucleophilic attack, while the descriptors σ_k^- and ω_k^- reflect a site's ability to produce electron density through electrophilic attack. In terms of the dual descriptor, it is an effective tool for forecasting efficiency and identifying issues related to regioselectivity. In fact, a positive dual descriptor indicates a position that is probably to accept electron density, making it further electrophilic. Contrarywise, a negative double descriptor suggests a location capable of generating electron density, reinforcing its nucleophilic character. A site with a dual descriptor value near zero indicates an equal ability to accept and provide electronic density. The local descriptor values are calculated using the following equations [46-49]:

$$f_k^+ = q_k(N+1) - q_k(N) \quad (9)$$

$$f_k^- = q_k(N) - q_k(N-1) \quad (10)$$

$$\sigma_k^+ = \sigma f_k^+ \quad (11)$$

$$\sigma_k^- = \sigma f_k^- \quad (12)$$

$$\omega_k^+ = \omega f_k^+ \quad (13)$$

$$\omega_k^- = \omega f_k^- \quad (14)$$

$$\eta_k^+ = \eta f_k^+ \quad (15)$$

$$\eta_k^- = \eta f_k^- \quad (16)$$

Where:

$q_k(N)$ is the electron population of the atom k in the neutral molecule.

$q_k(N+1)$ is the electron population of the atom k in the anionic molecule.

$q_k(N-1)$ is the electron population of the atom k in the cationic molecule.

The values of the dual descriptors are obtained through the subsequent equations [50-52].

$$\Delta f = f_k^+ - f_k^- \quad (17)$$

$$\Delta\sigma = \sigma_k^+ - \sigma_k^- \quad (18)$$

$$\Delta\omega = \omega_k^+ - \omega_k^- \quad (19)$$

All the results are summarized in tables 9-12 below

Table 9. *NBO charges for (I) computed with DFT/ RM062X/6-311^{++}G(d,p) method in gas and solvent phases.*

Atoms	(I) in gas phase			(I) in water			(I) in tetrahydrofuran (THF)		
	q(N)	q(N-1)	q(N+1)	q(N)	q(N-1)	q(N+1)	q(N)	q(N-1)	q(N+1)
O1	-0.53336	-0.46999	-0.31181	-0.53639	-0.20537	-0.32012	-0.53563	-0.47618	-0.31842
O2	-0.56065	-0.39709	-0.38437	-0.63017	-0.13050	-0.41971	-0.61698	-0.45751	-0.41318
O3	-0.58162	-0.55533	-0.29229	-0.57929	-0.27335	-0.29221	-0.58658	-0.57051	-0.29603
O4	-0.57973	-0.55064	-0.29714	-0.62658	-0.30323	-0.31862	-0.61039	-0.59029	-0.31042
C1	0.77962	0.74965	0.34921	0.79262	0.34976	0.32145	0.79033	0.76789	0.32745
C2	-0.30309	-0.18428	-0.34109	-0.31474	0.04652	-0.31964	-0.31245	-0.16755	-0.32442
C3	-0.11439	-0.12996	-0.25830	-0.09152	-0.09878	-0.29738	-0.09644	-0.10713	-0.29016
C4	-0.14627	-0.04456	-0.06660	-0.14306	0.08937	-0.05036	-0.14343	-0.02250	-0.05277
C5	0.35491	0.47528	0.12460	0.35158	0.36138	0.10857	0.35223	0.48672	0.11184
C6	-0.22437	-0.21621	-0.13673	-0.22777	-0.12955	-0.12445	-0.22677	-0.22181	-0.12674
C7	-0.19454	-0.12251	-0.26101	-0.19893	0.00942	-0.24761	-0.19814	-0.10453	-0.25041
C8	0.28574	0.43492	0.16657	0.28051	0.30544	0.16885	0.28301	0.41843	0.16947
C9	-0.19124	-0.21069	-0.21340	-0.18776	-0.14883	-0.21011	-0.18824	-0.20544	-0.21095
C10	0.83414	0.83262	0.41574	0.85488	0.43029	0.42756	0.85026	0.85070	0.42499
C11	-0.68336	-0.68734	-0.33992	-0.68700	-0.34308	-0.34353	-0.68512	-0.68437	-0.34249

Table 9. *Continued.*

Atoms	(I) in benzene			(I) in toluene		
	q(N)	q(N-1)	q(N+1)	q(N)	q(N-1)	q(N+1)
O1	-0.53436	-0.19076	-0.31548	-0.60952	-0.19175	-0.58218
O2	-0.59137	-0.10870	-0.40012	-0.69016	-0.09898	-0.58218
O3	-0.58792	-0.27062	-0.29643	-0.65029	-0.27263	-0.58575
O4	-0.59214	-0.28372	-0.30178	-0.69248	-0.29096	-0.61261
C1	0.78555	0.33982	0.33826	0.92877	0.33413	0.74432
C2	-0.30818	0.02414	-0.33297	-0.34388	0.03413	-0.45571
C3	-0.10521	-0.10344	-0.27590	-0.03853	-0.10174	-0.28178
C4	-0.14464	0.07342	-0.05837	-0.17075	0.07665	-0.12881
C5	0.35367	0.35840	0.11716	0.40352	0.35440	0.31055
C6	-0.22525	-0.11956	-0.13078	-0.22442	-0.12234	-0.25998
C7	-0.19600	-0.00791	-0.25553	-0.16227	-0.00285	-0.32170
C8	0.28538	0.32426	0.16892	0.30069	0.31554	0.28041
C9	-0.18950	0.32426	-0.21160	-0.15429	-0.15038	-0.27529
C10	0.84209	0.42322	0.42038	0.97617	0.42385	0.83905
C11	-0.68346	-0.34198	-0.34129	-0.61559	-0.34330	-0.68410

Table 10. *Reactivity descriptors calculated with natural charges for compound (I).*

Atoms	Local descriptors								Dual descriptors		
	f^-	f^+	σ^-	σ^+	η^-	η^+	ω^-	ω^+	Δf	$\Delta\sigma$	$\Delta\omega$
O1	-0.06337	0.22155	-0.00957	0.03345	-0.21039	0.73555	-0.21989	0.76878	0.28492	0.04302	0.98867
O2	-0.16356	0.17628	-0.02470	0.02662	-0.54302	0.58525	-0.56755	0.61169	0.33984	0.05132	1.17924
O3	-0.02629	0.28933	-0.00397	0.04369	-0.08728	0.96058	-0.09123	1.00398	0.31562	0.04766	1.09520
O4	-0.02909	0.28259	-0.00439	0.04267	-0.09658	0.93820	-0.10094	0.98059	0.31168	0.04706	1.08153
C1	0.02997	-0.43041	0.00453	-0.06499	0.09950	-1.42896	0.10400	-1.49352	-0.46038	-0.06952	-1.59752
C2	-0.11881	-0.038	-0.01794	-0.00574	-0.39445	-0.12616	-0.41227	-0.13186	0.08081	0.01220	0.28041
C3	0.01557	-0.14391	0.00235	-0.02173	0.05169	-0.47778	0.05403	-0.49937	-0.15948	-0.02408	-0.55340
C4	-0.10171	0.07967	-0.01536	0.01203	-0.33768	0.26450	-0.35293	0.27645	0.18138	0.02739	0.62939
C5	-0.12037	-0.23031	-0.01818	-0.03478	-0.39963	-0.76463	-0.41768	-0.79918	-0.10994	-0.01660	-0.38149
C6	-0.00816	0.08764	-0.00123	0.01323	-0.02709	0.29096	-0.02832	0.30411	0.0958	0.01447	0.33243
C7	-0.07203	-0.06647	-0.01088	-0.01004	-0.23914	-0.22068	-0.24994	-0.23065	0.00556	0.00084	0.01929
C8	-0.14918	-0.11917	-0.02253	-0.01799	-0.49528	-0.39564	-0.51765	-0.41352	0.03001	0.00453	0.10413
C9	0.01945	-0.02216	0.00294	-0.00335	0.06457	-0.07357	0.06749	-0.07690	-0.04161	-0.00628	-0.14439
C10	0.00152	-0.4184	0.00023	-0.06318	0.00505	-1.38909	0.00527	-1.45185	-0.41992	-0.06341	-1.45712
C11	0.00398	0.34344	0.00060	0.05186	0.01321	1.14022	0.01382	1.19172	0.33946	0.05126	1.17790

Table 11. *Reactivity descriptors calculated with natural charges for compound (I).in water.*

Atoms	Local descriptors								Dual descriptors		
	f^-	f^+	σ^-	σ^+	η^-	η^+	ω^-	ω^+	Δf	$\Delta\sigma$	$\Delta\omega$
O1	-0.33102	0.21627	-0.04932	0.03222	-1.11554	0.72883	-1.16883	0.76365	0.54729	0.08155	1.93248
O2	-0.49967	0.21046	-0.07445	0.03136	-1.68389	0.70925	-1.76433	0.74313	0.71013	0.10581	2.50747
O3	-0.30594	0.28708	-0.04559	0.04277	-1.03102	0.96746	-1.08027	1.01368	0.59302	0.08836	2.09395
O4	-0.32335	0.30796	-0.04818	0.04589	-1.08969	1.03783	-1.14175	1.08741	0.63131	0.09407	2.22916
C1	0.44286	-0.47117	0.06599	-0.07020	1.49244	-1.58784	1.56374	-1.66370	-0.91403	-0.13619	-3.22744
C2	-0.36126	-0.0049	-0.05383	-0.00073	-1.21745	-0.01651	-1.27561	-0.01730	0.35636	0.05310	1.25831
C3	0.00726	-0.20586	0.00108	-0.03067	0.02447	-0.69375	0.02564	-0.72689	-0.21312	-0.03175	-0.75253
C4	-0.23243	0.0927	-0.03463	0.01381	-0.78329	0.31240	-0.82071	0.32732	0.32513	0.04844	1.14803
C5	-0.0098	-0.24301	-0.00146	-0.03621	-0.03303	-0.81894	-0.03460	-0.85807	-0.23321	-0.03475	-0.82346
C6	-0.09822	0.10332	-0.01463	0.01539	-0.33100	0.34819	-0.34681	0.36482	0.20154	0.03003	0.71164
C7	-0.20835	-0.04868	-0.03104	-0.00725	-0.70214	-0.16405	-0.73568	-0.17189	0.15967	0.02379	0.56379
C8	-0.02493	-0.11166	-0.00371	-0.01664	-0.08401	-0.37629	-0.08803	-0.39427	-0.08673	-0.01292	-0.30624
C9	-0.03893	-0.02235	-0.00580	-0.00333	-0.13119	-0.07532	-0.13746	-0.07892	0.01658	0.00247	0.05854
C10	0.42459	-0.42732	0.06326	-0.06367	1.43087	-1.44007	1.49923	-1.50887	-0.85191	-0.12693	-3.00809
C11	-0.34392	0.34347	-0.05124	0.05118	-1.15901	1.15749	-1.21438	1.21279	0.68739	0.10242	2.42717

Table 12. *Reactivity descriptors calculated with natural charges for compound (I).in toluene.*

Atoms	Local descriptors								Dual descriptors		
	f^-	f^+	σ^-	σ^+	η^-	η^+	ω^-	ω^+	Δf	$\Delta\sigma$	$\Delta\omega$
O1	-0.41777	0.02734	-0.06225	0.00407	-1.39953	0.09159	-1.47180	0.09632	0.44511	0.06632	1.56812
O2	-0.59118	0.10798	-0.08809	0.01609	-1.98045	0.36173	-2.08273	0.38041	0.69916	0.10417	2.46314
O3	-0.37766	0.06454	-0.05627	0.00962	-1.26516	0.21621	-1.33050	0.22737	0.4422	0.06589	1.55787
O4	-0.40152	0.07987	-0.05983	0.01190	-1.34509	0.26756	-1.41455	0.28138	0.48139	0.07173	1.69594
C1	0.59464	-0.18445	0.08860	-0.02748	1.99204	-0.61791	2.09492	-0.64982	-0.77909	-0.11608	-2.74473
C2	-0.37801	-0.11183	-0.05632	-0.01666	-1.26633	-0.37463	-1.33173	-0.39398	0.26618	0.03966	0.93775
C3	0.06321	-0.24325	0.00942	-0.03624	0.21175	-0.81489	0.22269	-0.85697	-0.30646	-0.04566	-1.07966
C4	-0.2474	0.04194	-0.03686	0.00625	-0.82879	0.14050	-0.87159	0.14775	0.28934	0.04311	1.01934
C5	0.04912	-0.09297	0.00732	-0.01385	0.16455	-0.31145	0.17305	-0.32753	-0.14209	-0.02117	-0.50058
C6	-0.10208	-0.03556	-0.01521	-0.00530	-0.34197	-0.11913	-0.35963	-0.12528	0.06652	0.00991	0.23435
C7	-0.15942	-0.15943	-0.02375	-0.02376	-0.53406	-0.53409	-0.56164	-0.56167	-1E-05	0.00000	-0.00004
C8	-0.01485	-0.02028	-0.00221	-0.00302	-0.04975	-0.06794	-0.05232	-0.07145	-0.00543	-0.00081	-0.01913
C9	-0.00391	-0.121	-0.00058	-0.01803	-0.01310	-0.40535	-0.01377	-0.42628	-0.11709	-0.01745	-0.41251
C10	0.55232	-0.13712	0.08230	-0.02043	1.85027	-0.45935	1.94582	-0.48307	-0.68944	-0.10273	-2.42890
C11	-0.27229	-0.06851	-0.04057	-0.01021	-0.91217	-0.22951	-0.95928	-0.24136	0.20378	0.03036	0.71792

The local and dual descriptors of compound (I), calculated at the M062X /6-311^{++}G(d,p) level, indicate that the carbon atom C1 of compound (I) in water, in a sp^2 hybridization state, is the preferred site for electrophile attack, with a $\Delta\omega$ value of -3.22744. Based on the aforementioned level of calculation, a nucleophilic attack is predicted to occur on the O2 atom with a value of $\Delta\omega = 2.50747$. These local and dual descriptors results refine those obtained with Fukui functions, thanks to their precision [28].

3.3.4. Thermodynamic Parameters

The thermodynamic properties or parameters value (ΔS, ΔH and ΔG) provides insight into the spontaneity, randomness, and exothermic or endothermic nature of a process. To achieve these parameters, we need to know the entropy, enthalpy and free energy of the different compounds (reactants and products) of the synthesis reaction. For this reason, we have computed these standard thermodynamic quantities or parameters namely entropy S, heat capacity Cp, the enthalpy H and the free energy G from 25 K to 1000 K in steps of 25 K with the Perdew-Wang (PWC) functional and DND (Double-numerical + d-DNP) basis set of the DMol^3 module implemented in Materials Studio software. The results are summarized in table 13 and plotted in figure 14.

Table 13. *PWC/DND calculated of standard thermodynamic quantities (S(Cal.K^{-1}.mol^{-1}), Cp(Cal.K^{-1}.mol^{-1}), H((kcal.mol^{-1}), G(kcal.mol^{-1})) for compound (I).*

T(K)	S	C_p	H	G
25	55.757	11.433	103.617	102.223
50	65.087	15.67	103.959	100.705
75	72.048	18.801	104.391	98.987
100	77.864	21.798	104.898	97.112
125	83.064	24.956	105.482	95.099

T(K)	S	C_p	H	G
150	87.907	28.308	106.148	92.962
175	92.533	31.822	106.899	90.706
200	97.018	35.452	107.74	88.336
225	101.407	39.149	108..672	85.856
250	105..724	42.868	109.697	83.266
275	109.984	46.563	110.815	80.57
298.15	113.882	49.932	111.932	77.768
300	114.192	50.198	112.025	77.768
325	118.35	53.741	113.324	74.861
350	122.459	57.169	114.711	71.85
375	126.516	60.463	116.182	68.738
400	130.52	63.613	117.733	65.525
425	134.467	66.614	119.361	62.213
450	138.356	69.464	121.063	58.802
475	142.185	72.165	122.833	55.295
500	145.952	74.721	124.67	51.693
525	149.657	77.138	126.568	47.998
550	153.299	79.422	128.525	44.211
575	156.877	81.582	130.538	40.334
600	160.393	83.624	132.603	36.368
625	163.846	85.556	134.718	32.315
650	167.238	87.385	136.88	28.176
675	170.568	89.119	139.087	23.953
700	173.839	90.763	141.336	19.648
725	177.052	92.323	143.624	15.262
750	180.207	93.806	145.951	10.796
775	183.306	95.216	148.314	6.252
800	186.35	96.557	150.711	1.631
825	189.341	97.835	153.141	-3.065
850	192.28	99.053	155.603	-7.836
875	195.168	100.215	158.094	-12.679
900	198.007	101.324	160.613	-17.594
925	200.798	102.383	163.159	-22.579
950	203.542	103.395	165.732	-27.633
975	206.24	104.362	168.329	-32.755
1000	208.894	105.288	170.949	-37.945

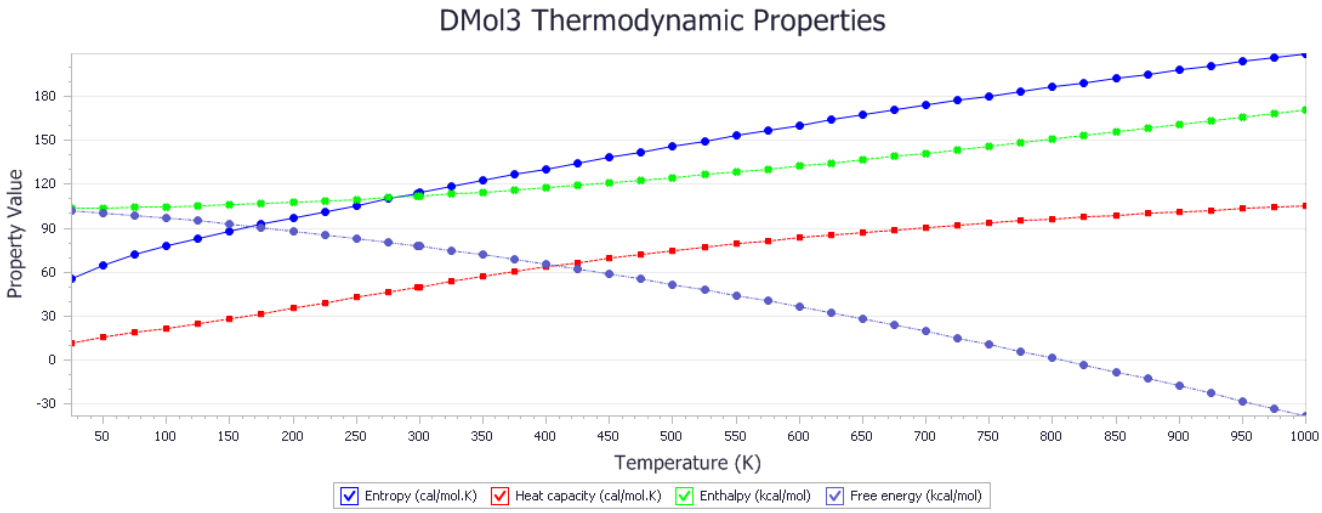

Figure 14. *Thermodynamic property curves with entropy in cal/mol, heat capacity in cal/mol.K, enthalpy and free energy in kcal/mol.*

4. Conclusion

In this paper, spectroscopic and X-ray crystallographic methods were used to solve and refine the molecular structure of the title compound (I). The intermolecular interactions present in the structure, the geometrical parameters as well as the conformations were analyzed using the versatile crystallographic tool Platon [17]. The resulting bond lengths, bond angles, and torsion angles were confronted to the corresponding calculated data. The comparatively analysis showed no substantial differences between the experimental and theoretical structures. Furthermore, we conducted an investigation into the molecular electrostatic potential and HOMO-LUMO analysis for Coumarin-6-yl acetate utilizing DFT/ M062X /6-311^{++}G(d,p) calculations. The MEP maps highlighted the nucleophilic sites around the oxygen atoms O2 and O4 and are materialized by the zones marked in red color (negative potential zone), while positive potential sites were found in proximity to the hydrogen atoms. This information provides insight into the regions where intra- and intermolecular interactions could potentially be observed. Furthermore, the reactivity descriptors of (I) were estimated via PWC/DND methods. The overall descriptors show that compound (I) in the benzene solvent demonstrates optimal stability, exhibiting an energy gap value of 9.48 eV. In contrast, compound (I) in the gaseous phase exhibits the lowest energy gap value (ΔEg = 6.64 eV), indicating that it is the least stable among the five mixtures of (I) with the solvents. In addition, the local and dual descriptors of compound (I) indicate that the carbon atom C1 of compound (I) in water is the optimal site for electrophile attack, with a Δω value of -3.22744. Based on the aforementioned level of calculation, it is predicted that a nucleophilic attack will occur on the O2 atom with a value of Δω = 2.50747 that seem to the best prevision because of the best accuracy of the method [28]. These findings, derived from the electrophilic or nucleophilic attack zone approach, will facilitate precise regulation of chemical reactions, thereby enabling the realization of desired molecular structures. The standard thermodynamic quantities or parameters namely entropy S, heat capacity Cp, the enthalpy H and the free energy G have also been performed from 25 K to 1000 K in steps of 25 K. The obtained results at 298.15K and 1 Pa are S = 113.882 Cal.K^{-1}.mol^{-1}, C_p = 49.932 Cal.K^{-1}.mol^{-1}, H = 111.932 kcal.mol^{-1} and G = 77.768 kcal.mol^{-1}.

Abbreviations

ESI-MS	ElectroSpray Ionization Mass Spectrometry
FT-IR	Fourier Transform Infrared Spectroscopy
^{1}H NMR	Proton Nuclear Magnetic Resonance
^{13}C NMR	Carbon-13 (C13) Nuclear Magnetic Resonance
B3LYP	Becke, 3-parameter, Lee–Yang–Parr
THF	TetraHydroFuran
NBO	Natural Bond Orbital
HOMO	Highest Occupied Molecular Orbital
LUMO	Lowest unoccupied molecular orbital
CFIA	Canadian Food Inspection Agency
ADI	Acceptable Daily Intake
EFSA	European Food Safety Authority
NLO	Non-Linear Optical
XRD	X-ray Diffraction
3D	Three-Dimensional
FMO	Frontier Molecular Orbitals
FF	Fukui Function
PWC	Perdew-Wang
DND	Double-numerical + d
TMS	Tetramethylsilane
DFT	Density Functional Theory
HSQC	Heteronuclear Single-Quantum Correlation

ATR	Attenuated Total Reflectance
APT	Attached Proton Test
CDCl3	Deuterated Chloroform
RMSD	Root Mean Square Deviations
MEP	Molecular Electrostatic Potential

Acknowledgments

The authors thank the Spectropole Service of the Federation of Chemical Sciences (Aix-Marseille University, France) for conducting the complete analysis.

Author Contributions

Honoré Kouadio Yao: Funding acquisition, Validation, Writing – original draft

Zakaria Koulabiga: Validation, Synthesis

Akoun Abou: Conceptualization, Investigation, Methodology, Supervision, Validation, Writing – review & editing

Abdoulaye Djandé: Conceptualization, Project administration, Supervision, Validation, Writing – review & editing

Stéphane Coussan: Data curation, Formal Analysis, Project administration, Resources, Software, Supervision, Validation, Visualization

Olivier Ouari: Data curation, Formal Analysis, Project administration, Resources, Software, Validation, Visualization

Conflicts of Interest

The authors declare no conflicts of interest.

References

[1] Matos, M. J., Santana, L., Uriarte, E., Abreu, O. A., Molina, E., & Yordi, E. G. (2015). *Coumarins — An Important Class of Phytochemicals. Phytochemicals - Isolation, Characterisation and Role in Human Health.* (pp. 113-140). Royaune-Uni: IntechOpen. https://doi.org/10.5772/59982

[2] Zeng, L., Zhang, R.-Y., Meng, T., Lou, Z.-C. (1990). Determination of nine flavonoids and coumarins in licorice root by high-performance liquid chromatography. *J. Chromatogr. A*, 513, 247-254. https://doi.org/10.1016/S0021-9673(01)89441-3

[3] Shojaii, A., Fard, M. H., 2012. Review of pharmacological properties and chemical constituents of Pimpella anisum. *ISRN Pharmaceutics*, 2012, 510795. https://doi.org/10.5402/2012/510795

[4] Abraham, K., Wöhrlin, F., Lindtner, O., Heinemeyer, G., Lampen, A., 2010. Toxicology and risk assessment of coumarin: Focus on human data. *Mol. Nutr. Food Res*, 54(2), 228-239. https://doi.org/10.5402/2012/510795

[5] Lake, B. G. (1999). Coumarin metabolism, toxicity and carcinogenicity: Relevance for human risk assessment. *Food and Chemical Toxicology*, 37(4), 423-453. https://doi.org/10.1016/s0278-6915(99)00010-1

[6] Coumarin in flavourings and other food ingredients with flavouring properties. Scientific opinion of the panel on food additives, flavourings, processing aids and materials in contact with food (AFC). (2008*). EFSA Journal*, 793, 1-15. https://doi.org/10.2903/j.efsa.2008.793

[7] Basanagouda M, Kulkarni M V, Sharma D, Gupta V K, Pranesha P, Sandhyarani P and Rasal V P., (2009). *J. Chem. Sci.* 121, 485–495. https://doi.org/10.1007/s12039-009-0058-z

[8] Vuković N, Sukdolak S, Solujić S and Niciforović N, (2010). An efficient synthesis and antioxidant properties of novel imino and amino derivatives of 4-hydroxy coumarins. *Arch. Pharm. Res.* 33; 5–15. https://doi.org/10.1007/s12272-010-2220-z

[9] Emmanuel-Giota A A, Fylaktakidou K C, Litinas K E, Nicolaides D N and Hadjipavlou-Litina D J,. (2001). Synthesis and biological evaluation of several 3-(coumarin-4-yl) tetrahydroisoxazole and 3-(coumarin-4-yl) dihydropyrazole derivatives. *Heterocycl. Chem.*; 38: 717–722. https://doi.org/10.1002/jhet.5570380329

[10] D. R. Kanis, M. A. Ratner, T. J. Marks, (1994). Design and construction of molecular assemblies with large second-order optical nonlinearities. Quantum chemical aspects. *Chem. Rev.* 94, 195–242. https://doi.org/10.1021/cr00025a007

[11] D. J. Williams, (1992). Non-linear optical properties of organic materials. *Thin Solid Films* 216, 117–122 https://doi.org/10.1016/0040-6090(92)90879-G

[12] P. J. Mendes, J. P. Prates Ramalho, A. J. E. Candeias, M. P. Robalo, M. H. Garcia, (2005). Density functional theory calculations on η^5 - monocyclopentadienylnitrilecobalt complexes concerning their second-order nonlinear optical properties. *J. Mol. Struct. (Theochem.)* 729 109–113 https://doi.org/10.1016/j.theochem.2004.12.048

[13] N. M. F. S. A. Cerqueira, A. M. F. Oliveira-Campos, P. J. Coelho, L. H. Melo de Carvalho, A. Samat, R. Guglielmetti, (2005). Synthesis of Photochromic Dyes Based on Annulated Coumarin Systems. *Helv. Chim. Acta* 85, 442–450. ttps://doi.org/10.1002/1522-2675(200202)85:2<442::AID-HLCA442>3.0.CO;2-9

[14] S. P. G. Costa, J. Griffiths, G. Kirsch, A. M. F. Oliveira-Campos. Synthesis of thieno[2,3-d]thiazole derived dyes with potential application in nonlinear optics. *Ann. Quum. Int.* Ed. (1998), 94, 186–188. https://www.researchgate.net/publication/298841639_Synthesis_of_thieno23-dthiazole_derived_dyes_with_potential_application_in_nonlinear_optics/link/5b83a77392851c1e1234b3b0/download?_tp=eyJjb250ZXh0Ijp7ImZpcnN0UGFnZSI6InB1YmxpY2F0aW9uIiwicGFnZSI6InB1YmxpY2F0aW9uIn19

[15] M. M. M. Raposo, A. M. R. C. Sousa, A. M. C. Fonseca, G. Kirsch, (2005). Thienylpyrrole Azo Dyes: Synthesis, Solvatochromic and Electrochemical Properties. *Tetrahedron* 61, 8249–8256. https://doi.org/10.1016/j.tet.2005.06.039

[16] N. Arumugam, A. I. Almansour, R. S. Kumar, V. S. Krishna, D. Sriram, N. Dege. (2021). Stereoselective synthesis and discovery of novel spirooxindolopyrrolidine engrafted indandione heterocyclic hybrids as antimycobacterial agents. *Bioorg. Chem.*, 110, 104798. https://doi.org/10.1016/j.bioorg.2021.104798

[17] Spek, A. L., 2009. Structure validation in chemical crystallography. *Acta Cryst.*, D65, 148–155. https://doi.org/10.1107/S090744490804362X

[18] Frisch M. J., Trucks G. W., Schlegel H. B., Scuseria G. E., Robb M. A., Cheeseman J. R., et al.; (2013) GAUSSIAN09. Gaussian, Inc., Wallingford, CT, USA.

[19] B. Delley, (1990). An All-Electron Numerical Method for Solving the Local Density Functional for Polyatomic Molecules. *J. Chem. Phys.* 92, 508-517. https://doi.org/10.1063/1.458452

[20] B. Delley, (2000). From Molecules to Solids with DMol3. *J. Chem. Phys.* 113, 7756-7764. https://doi.org/10.1063/1.1316015

[21] Tse-Lok, H., (1975). Hard soft acids bases (HSAB) principle and organic chemistry. *Chem. Rev.* 75(1), 1-20. https://doi.org/10.1021/cr60293a001

[22] R. G. Pearson, (1963). Hard and Soft Acids and Bases. J. *Amer. Chem. Soc*, 85(22), 3533-3539. https://doi.org/10.1021/ja00905a001

[23] Abou A, Sosso S., Kouassi A. F., Zoueu T. J., Djand éA., Ouari O. (2021) Synthesis, Characterization, Crystal Structure and Quantum Chemical Calculations of 2-oxo-2H-chromen-3-yl Acetate. Sci. J. Chem., 9(2), 29-44 https://doi.org/10.11648/j.sjc.20210902.11

[24] Rigaku OD (2015). CrysAlis PRO. Rigaku Oxford Diffraction, Yarnton, England. https://rigaku.com/products/crystallography/x-ray-diffraction/crysalispro

[25] Burla M C, Caliandro R, Carrozzini B, Cascarano G L, Cuocci C, Giacovazzo C, Mallamo M, Mazzone A and Polidori G, (2015). Crystal structure determination and refinement *via SIR2014*. *J. Appl. Cryst.* 48, 306–309. https://doi.org/10.1107/S1600576715001132

[26] Farrugia L J., (2012). WinGX and ORTEP for Windows: An Update. *J. Appl. Cryst.* 45, 849–854. http://dx.doi.org/10.1107/S0021889812029111

[27] Sheldrick G M., (2015). Crystal Structure Refinement with SHELXL. *Acta Cryst.* C71, 3–8. https://journals.iucr.org/c/issues/2015/01/00/fa3356/fa3356.pdf

[28] Martinez-Araya J. I., (2014). Why is the dual descriptor a more accurate local reactivity descriptor than Fukui functions? *J. Math. Chem.* 53(2), 451 - 465. https://doi.org/10.1007/s10910-014-0437-7

[29] Canevet, D., Salle, M., Zhang, G., Zhang, D., and Zhu, D., (2009). Tetrathiafulvalene (TTF) derivatives: key building-blocks for switchable processes. *Chem. Comm.* 17, 2245-2269. https://doi.org/10.1039/B818607N

[30] Vektariene, A., Vektaris, G., and Svoboda, J., (2009). A theoretical approach to the nucleophilic behavior of benzofused thieno [3,2-b] furans using DFT and HF based reactivity descriptors, Arkivoc: Online Journal of Organic Chemistry. *ARKIVOC*. vii, 311-329. https://www.researchgate.net/publication/229077420

[31] Islam, M. J., Kumer, A., Sarker, N., Paul, S., and Zannat, A., (2019). The prediction and theoretical study for chemical reactivity, thermophysical and biological activity of morpholinium nitrate and nitrite ionic liquid crystals: A DFT study. *Adv. J. Chem. A* 2(4), 316-326. https://www.researchgate.net/publication/333081305_The_prediction_and_theoretical_study_for_chemical_reactivity_thermophysical_and_biological_activity_of_morpholinium_nitrate_and_nitrite_ionic_liquid_crystals_A_DFT_study https://doi.org/10.33945/SAMI/AJCA.2019.4.5

[32] E. AlShamaileh, (2014). DFT Study of Monochlorinated Pyrene Compounds. *Comput. Chem.* 2, 43-49. https://doi.org/10.4236/cc.2014.23006

[33] Flores-Holgu ń, N., Frau, J., and Glossman-Mitnik, D., (2019). Chemical reactivity and bioactivity properties of the Phallotoxin family of fungal peptides based on Conceptual Peptidology and DFT study. *Heliyon*, 5(8), e02335. https://doi.org/10.1016/j.heliyon.2019.e02335

[34] Abbaz, T., Bendjeddou, A., and Villemin, D., (2018). Molecular structure, HOMO, LUMO, MEP, natural bond orbital analysis of benzo and anthraquinodimethane derivatives. *Pharmaceutical and Biological Evaluations*, 5(2), 27-39. https://doi.org/10.26510/2394-0859.pbe.2018.04

[35] El_Kalai F., Çınar E. B., Lai C. H., Said Daoui S., Chelfi T., Allali M., Dege N., Karrouchi K., Benchat N., (2020). Synthesis, spectroscopy, crystal structure, TGA/DTA study, DFT and molecular docking investigations of (E)-4-(4-methylbenzyl) -6-styrylpyridazin-3(2H)-one, *J. Mol. Struct.*, 129435 https://doi.org/10.1016/j.molstruc.2020.129435

[36] Agrahari B., Layek S., Ganguly R, Dege N., Pathak D. D. (2019). Synthesis, characterization and single crystal X-ray studies of pincer type Ni(II)-Schiff base complexes: Application in synthesis of 2-substituted benzimidazoles. *J. Organomet. Chem.*, 890, 13-20. https://doi.org/10.1016/j.jorganchem.2019.03.018

[37] Abou A., Yoda J., Djand é A., Coussan S. and Zoueu T J. (2018). Crystal structure of 2-oxo-2H-chromen-7-yl 4-fluorobenzoate. *Acta Cryst.* E74, 761–765. https://doi.org/10.1107/S205698901800614X

[38] Abou A., Sosso S., Kouassi A F., Zoueu T J., Djandé A., Ouari O. (2021). Synthesis, Characterization, Crystal Structure and Quantum Chemical Calculations of 2-oxo-2H-chromen-3-yl Acetate. *Sci. J. Chem.* 9(2), 29-44 https://doi.org/10.11648/j.sjc.20210902.11

[39] Koulabiga Z., Yao K H., Abou A., Djandé A., Giorgi M., Coussan S. (2024). Synthesis, Characterization, Hirshfeld Surface Analysis and Quantum Chemical Calculations of 2-oxo-2H- Chromen-6-yl 4-Methoxybenzoate. *Am. J. Org. Chem.*, 12(1): 1-19. https://doi.org/10.5923/j.ajoc.20241201.01

[40] Janiak J, *J. (2000).* A critical account on π–π stacking in metal complexes with aromatic nitrogen-containing ligands. *Chem. Soc. Dalton Trans.* 3885–3896. https://doi.org/10.1039/B003010O

[41] D. L. Beveridge; R. Lavery Theoretical Biochemistry and Molecular Biophysics: DNA. Proteins, Adenine Press, 1990. https://doi.org/10.1080/07391102.1990.10507839

[42] Politzer P. and J. S. Murray J. S.; (2002). The fundamental nature and role of the electrostatic potential in atoms and molecules. *Theor. Chem. Acc.* 108(3), 134–142. https://doi.org/10.1007/s00214-002-0363-9

[43] Pearson, R. G. (1986). Absolute electronegativity and hardness correlated with molecular orbital theory. *Proc. Natl. Acad. Sci. U.S.A.* Nov;. 83(22): 8440-8441. https://doi.org/10.1073/pnas.83.22.8440

[44] Pearson, R. G. (1963) Hard and Soft Acids and Bases. *J. Am. Chem. Soc.* 85, 3533-3539. https://doi.org/10.1021/ja00905a001

[45] Yang, W., Parr, R. G. and Pucci, R. (1984). Electron Density, Kohn-Sham Frontier Orbitals, and Fukui Functions. *J. Chem. Phys.* 81, 2862-2863. https://doi.org/10.1063/1.447964

[46] Yang, W. and Mortier, W. (1986) The Use of Global and Local Molecular Parameters for the Analysis of the Gas-Phase Basicity of Amines. *J. Am. Chem. Soc*. 108, 5708-5711. https://doi.org/10.1021/ja00279a008

[47] Yang, W. and Parr, R. G. (1985). Chemistry. Hardness, Softness, and the Fukui Function in the Electronic Theory of Metals and Catalysis. Proceedings of the National Academy of Sciences of the United States of America, 82, 6723-6726. https://doi.org/10.1073/pnas.82.20.6723

[48] Chattaraj, P. K., Maiti, B. and Sarkar, U. (2003) Philicity: A Unified Treatment of Chemical Reactivity and Selectivity. *J. Phys. Chem. A* 107, 4973-4975. https://doi.org/10.1021/jp034707u

[49] Fuentealba, P. and Contreras, R. (2002). Fukui Function in Chemistry. In: Sen, K. D., Ed., Reviews in Modern Quantum Chemistry: A Celebration of the Contributions of Robert G Parr, World Scientific, River Edge, 1013-1052. https://doi.org/10.1002/chin.200329281

[50] Padmanabhan, J., Parthasarathi, R., Elango, M., Subramanian, V., Krishnamoorthy, B. S., Gutierrez-Oliva, S., Toro-Labbe, A., Roy, D. R. and Chattaraj, P. K. (2007) Multiphilic Descriptor for Chemical Reactivity and Selectivity. *J. Phys. Chem.* 111, 9130-9138. https://doi.org/10.1021/jp0718909

[51] Morell, C., Grand, A. and Toro-Labbé, A. (2005). New Dual Descriptor for Chemical Reactivity. *J. Phys. Chem.* 109, 205-212. https://doi.org/10.1021/jp046577a

[52] Morell, C., Grand, A. and Toro-Labbé, A. (2006) Theoretical Support for Using the Delta f(r). Descriptor *Chem. Phys. Lett.* 425, 342-346. https://doi.org/10.1016/j.cplett.2006.05.003